Research Article | Open Access

Intelligence & Robotics

Liang *et al. Intell. Robot.* **2026**, *6*(2), 229-52 **DOI:** 10.20517/ir.2026.12

Fixed-time prescribed performance formation control of heterogeneous UAV-USV systems under actuator faults

Zihao Liang[1], Weixiang Zhou[1], Yandan Wang[2], Yayu Yang[3]

Keywords:
Heterogeneous multi-agent systems, UAV-USV cooperation, fixed-time control, prescribed performance control, fault tolerance control

Citation: Liang, Z.; Zhou, W.; Wang, Y.; Yang, Y. Fixed-time prescribed performance formation control of heterogeneous UAV-USV systems under actuator faults. *Intell. Robot.* **2026**, *6*(2), 229-52. http://dx.doi.org/10.20517/ir.2026.12

Received: 22 Dec 2025
First Decision: 27 Feb 2026
Revised: 1 Apr 2026
Accepted: 30 Apr 2026
Published: 25 May 2026

Academic Editors:
Simon Yang, Huaicheng Yan
Copy Editor:
Pei-Yun Wang
Production Editor:
Pei-Yun Wang

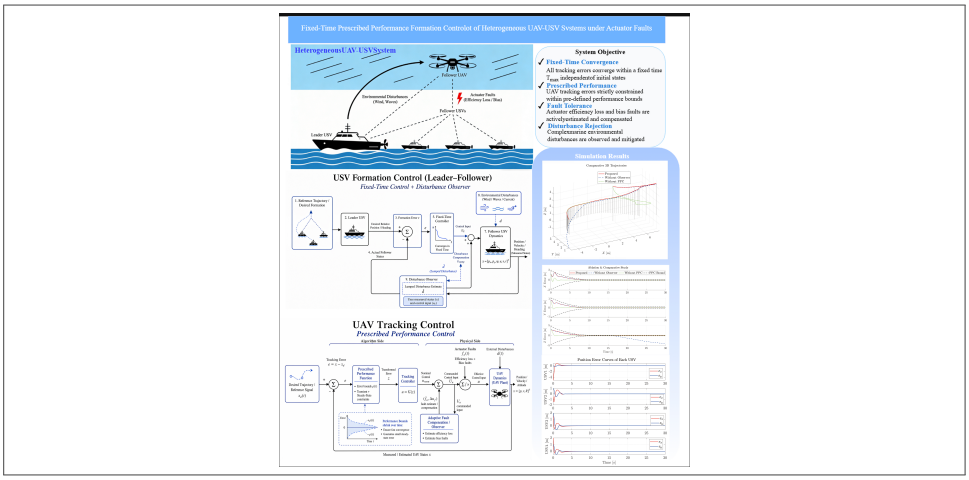

Abstract

This paper addresses the robust cooperative control problem of heterogeneous unmanned aerial vehicles (UAVs) and unmanned surface vehicles (USVs) under actuator faults and complex environmental disturbances. A heterogeneous fixed-time prescribed performance formation control framework is proposed to ensure precise coordination among the vehicles. Specifically, a disturbance observer-based fixed-time control law is developed for USV formation control, employing a leader-follower topology. Simultaneously, a fixed-time prescribed performance control strategy based on error transformation is designed for the UAVs to ensure convergence within specified performance boundaries. To enhance system resilience, a disturbance observer is designed for the USV formation system to handle complex marine environmental disturbances. Meanwhile, for the UAV subsystem, an adaptive fault-tolerant mechanism is integrated to estimate and compensate for loss of actuator efficiency and bias faults. Lyapunov stability analysis theoretically proves that all tracking errors in the closed-loop system converge to a small neighborhood of the origin within a fixed time,

[1]College of Information Engineering, Shanghai Maritime University, Shanghai 201306, China.
[2]School of Intelligent Manufacturing, Nantong College of Science and Technology, Nantong 226007, Jiangsu, China.
[3]Department of Electrical Engineering and Computer Science, The University of Tennessee, Knoxville, TN 37996, USA.

Correspondence to: Yandan Wang, School of Intelligent Manufacturing, Nantong College of Science and Technology, Nantong 226007, Jiangsu, China. E-mail: ydwang_ncst@163.com

independent of the initial system states. The simulation results validate the effectiveness of the proposed formation methods.

1. INTRODUCTION

Unmanned systems have become crucial components in military and civilian applications, as well as in rescue and detection operations, owing to the rapid development of automation technologies[1,2]. Their primary advantages lie in reducing human intervention, improving system autonomy, mitigating operational risks, and ensuring personnel safety. With the constant growth of automation technologies for unmanned surface vehicles (USVs), the role of USVs in marine equipment ecosystems and civilian/military applications has become increasingly significant[3,4].

Although individual unmanned systems have advantages in particular missions, their operational capability and effectiveness are inherently restricted[5,6]. Therefore, researchers are increasingly focusing on the cooperative formation control of multiple unmanned systems to enhance multi-task collaboration capabilities. The most significant issue in USV formation control is the acquisition and processing of information. Collaborative formation is usually based on state information [via Global Navigation Satellite System (GNSS)/Inertial Navigation System (INS)] and neighbor information (via radar/SLAM), both of which are often limited by environmental adaptability, line-of-sight, and signal coverage[7].

In contrast, unmanned aerial vehicles (UAVs) possess distinct operational advantages, such as high maneuverability, rapid response capability, and most importantly, a wide and unobstructed top-down view[8,9]. When UAVs are integrated with USVs, the resulting heterogeneous UAV-USV system combines the complementary strengths of both domains: the UAV serves as an aerial monitor providing a global view, while the USV formation functions as a mobile base offering endurance and payload support[10]. Such cross-domain cooperation can significantly improve the autonomy and operational effectiveness of maritime missions[11,12].

Nevertheless, despite extensive research on cooperative control, achieving reliable formation control under harsh marine conditions remains challenging. In general, available control methods can be categorized into three groups according to their design objectives and operational characteristics:

First, regarding convergence performance, traditional cooperative controls largely rely on asymptotic stability or finite-time stability. For example, studies in[13,14] addressed consensus problems and derived sufficient conditions for exponential or asymptotic convergence. Although these methods are theoretically sound, the settling time is heavily dependent on the initial states of the system[15–17]. In emergency maritime rescue scenarios, where initial position errors are often random and large, such dependence can lead to unacceptable long convergence times[18]. Although finite-time control provides improved performance, the upper limit of the settling time still depends on the initial conditions. In contrast, fixed-time stability ensures that the settling time is bounded by a constant independent of the initial states. Recent advancements in this field have been achieved in the case of general multi-agent systems (MASs). As an illustration, earlier work has already examined fixed-time group consensus for MASs with nonlinear dynamics and uncertainties[19], and formulated fixed-time group tracking control methods to address unknown underlying nonlinear dynamics[20]. Although these sophisticated methods offer a solid theoretical basis for handling nonlinearities and uncertainties, their application to heterogeneous cross-domain marine systems (e.g., UAV-USV), particularly in the presence of simultaneous actuator failures and stringent performance requirements, remains insufficiently explored[21].

Second, regarding constraint handling and safety, optimization-based methods such as model predictive control (MPC) and control barrier functions (CBFs) are widely used. Studies in[22,23] have shown the usefulness

of MPC and CBF in constraint handling and collision avoidance. However, these methods are computationally intensive and require accurate global models, which can be impractical when considering resource-limited embedded systems. Prescribed performance control (PPC) provides a computationally efficient alternative by converting constrained tracking errors into unconstrained forms. Although a recent review[24] examined the concept of PPC in UAV-USV systems, further investigation is still required to guarantee strictly limited transient performance in heterogeneous systems under fault conditions.

Third, regarding robustness against faults and disturbances, marine systems are subject to various sources of uncertainty. Traditional robust control approaches generally treat actuator failures and environmental forces as bounded lumped disturbances[25,26]. Such passive approaches are conservative because the controller cannot actively identify particular actuator faults (e.g., efficiency loss[27] or bias) and thus cannot provide specific compensation, which can cause formation degradation[28,29]. Although some disturbance observers[30] and resilient control mechanisms[31–33] have been proposed, effective methods specifically designed to address complex hydrodynamic coupling and heterogeneous faults in UAV-USV systems remain insufficiently investigated[34–38].

Motivated by the above observations, this paper addresses the problem of **heterogeneous UAV-USV formation control subject to strict time constraints, actuator faults, and environmental disturbances.** A hierarchical leader-follower architecture[39] is adopted, where the USV formation acts as a mobile reference, while the UAV tracks the center of the formation. The objective is to design a unified control framework that guarantees: (1) Formation establishment within a user-defined fixed time; (2) Strict adherence to safety performance bounds; and (3) Active resilience against mechanical failures and environmental interference.

The main contributions of this paper are summarized as follows:

1. **A Heterogeneous Fixed-Time Control Framework:** An inclusive cooperative control framework is designed to integrate leader-follower fixed-time convergence control for the USV subsystem with fixed-time PPC for the UAV subsystem. The proposed framework guarantees accurate USV formation geometry and effective UAV tracking of the formation center within a predictable time, irrespective of the initial errors.

2. **Active Fault Tolerance with Disturbance Decoupling:** By integrating adaptive estimation with disturbance observers, the proposed method actively distinguishes and compensates for actuator efficiency loss/bias faults and lumped environmental disturbances. This strategy significantly reduces the conservatism compared to passive robust controls.

3. **Guaranteed Transient Performance:** By introducing prescribed performance functions (PPFs) and error transformation techniques, the transient overshoot and steady-state tracking errors of the UAV are strictly constrained within predefined boundaries, ensuring safe cross-domain tracking.

4. **Robust USV Formation:** A fixed-time disturbance observer is specifically employed for the USV subsystem to counteract harsh environmental disturbances, ensuring the stability of the mobile base.

2. METHODS

Before presenting the dynamic models, the control objectives and constraints are explicitly defined to clarify the research motivation. Consider a heterogeneous system composed of N follower USVs and 1 follower UAV, with a leader USV providing the reference trajectory. Let $\boldsymbol{\eta}_i$ and $\boldsymbol{\eta}_{d,i}$ denote the actual and desired positions of the i-th USV, respectively. Let $e_{a,k}$ [where $k \in \{x, y, z\}$] denote the UAV tracking error along each axis relative to the formation center.

The primary control objective is to design distributed control laws τ_i for the USVs and U_{uav} for the UAV, such that the following operational requirements are simultaneously satisfied:

1. **Objective 1: Fixed-Time Formation Convergence.** The position tracking error of the USV formation must converge to a small neighborhood of the origin within a user-defined fixed time T_{max}, independent of the initial system states. Mathematically, this is expressed as:
$$\lim_{t \to T_{max}} \|\boldsymbol{\eta}_i(t) - \boldsymbol{\eta}_{d,i}(t)\| \leq \epsilon_1, \quad \forall \boldsymbol{\eta}_i(0) \in \mathbb{R}^3 \tag{1}$$
where ϵ_1 is a sufficiently small positive constant.

2. **Objective 2: Prescribed Performance Constraint (Safety).** For the UAV, to ensure flight safety and transient performance, the tracking error $e_{a,k}(t)$ must strictly evolve within a predefined "funnel" envelope bounded by the performance function $\rho_k(t)$:
$$-\delta_k \rho_k(t) < e_{a,k}(t) < \delta_k \rho_k(t), \quad \forall t \geq 0 \tag{2}$$
where $\delta_k \in (0, 1]$ is a tuning parameter and $\rho_k(t)$ is a strictly decreasing positive function.

3. **Objective 3: Active Fault Tolerance.** The heterogeneous system must maintain stability and performance despite the presence of time-varying actuator faults. The fault model is defined as:
$$u_k(t) = \rho_k(t) U_k(t) + c_k(t) \tag{3}$$
where $\rho_k \in (0, 1]$ represents the unknown efficiency loss factor, and c_k denotes the unknown bias fault. The controller must adaptively estimate and compensate for these faults online.

Assumption 1. The desired trajectory of the leader USV and the formation geometry are smooth and bounded, and their time derivatives exist and remain bounded.

2.1. USV model

Consider a heterogeneous system consisting of one leader USV, multiple follower USVs, and one follower UAV. The coordinate systems of the heterogeneous UAV-USV cooperative system are illustrated in Figure 1. Let the position vector of the i-th USV in the inertial coordinate system be defined as $\boldsymbol{\eta}_i = [x_i, y_i, \psi_i]^T$, where x_i, y_i, and ψ_i represent the position coordinates and heading angle, respectively. The velocity vector in the body-fixed coordinate system is defined as $\boldsymbol{v}_i = [u_i, v_i, r_i]^T$, where u_i, v_i, and r_i represent the surge velocity, sway velocity, and yaw rate, respectively. The kinematic model of the USV is given by:
$$\dot{\boldsymbol{\eta}}_i = \boldsymbol{R}(\psi_i) \boldsymbol{v}_i \tag{4}$$

The rotation matrix is expressed as follows:
$$\boldsymbol{R}(\psi_i) = \begin{bmatrix} \cos\psi_i & -\sin\psi_i & 0 \\ \sin\psi_i & \cos\psi_i & 0 \\ 0 & 0 & 1 \end{bmatrix} \tag{5}$$

The dynamics equation is given by:
$$\boldsymbol{M}_i \dot{\boldsymbol{v}}_i + \boldsymbol{C}_i(\boldsymbol{v}_i)\boldsymbol{v}_i + \boldsymbol{D}_i \boldsymbol{v}_i = \boldsymbol{\tau}_i + \boldsymbol{\delta}_i \tag{6}$$

Remark 1 (Justification of the asymmetric fault-tolerant strategy for heterogeneous systems):
In this study, the fault-tolerant strategy is designed asymmetrically, which is entirely consistent with the heterogeneous nature of the UAV-USV cooperative system. In such a heterogeneous framework, the agents exhibit fundamentally different dynamic sensitivities and vulnerabilities, necessitating tailored resilient mechanisms. On one hand, UAVs are highly dynamic and rely entirely on continuous active thrust to counteract gravity; even minor degradation in actuator efficiency can lead to immediate altitude divergence and catastrophic failure (as demonstrated in the simulations). Therefore, the UAV subsystem strictly requires an **active fault-tolerant**

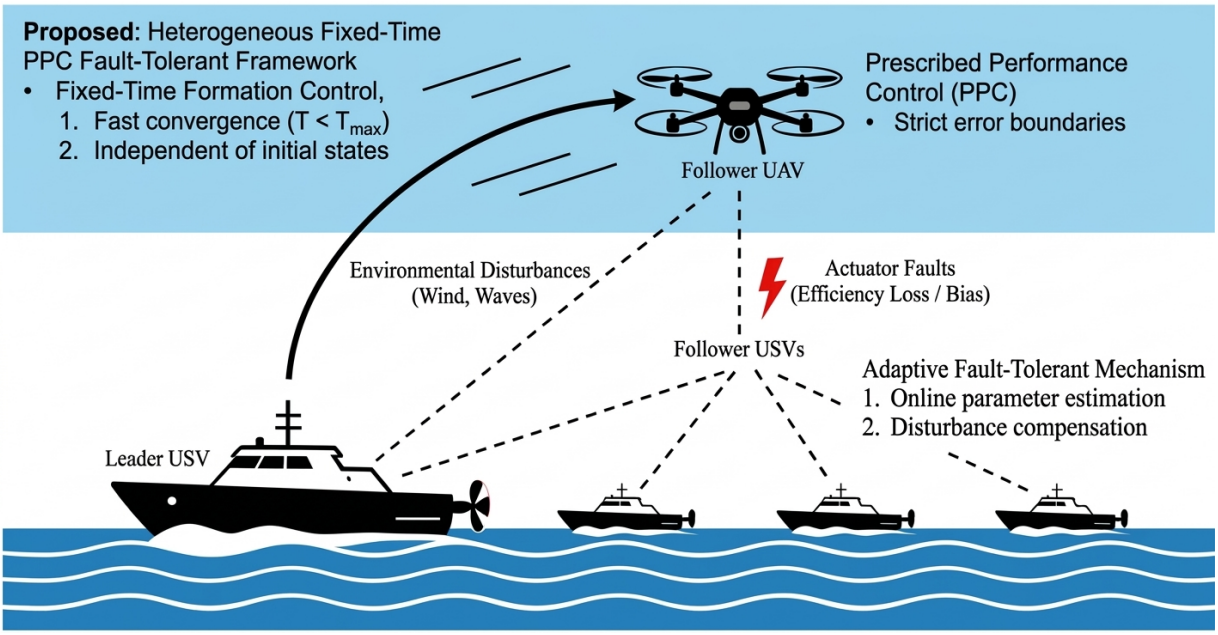

Figure 1. Overall framework of the heterogeneous UAV-USV formation system under complex marine environments, illustrating the leader-follower topology, environmental disturbances (wind, waves), and actuator faults affecting the agents. UAV: Unmanned aerial vehicle; USV: unmanned surface vehicle.

strategy, where actuator faults (efficiency loss and bias) are explicitly modeled and adaptively compensated. On the other hand, USVs are supported by natural buoyancy, operate at low speeds, and possess inherently large inertia. Minor actuator degradation in USVs manifests as sluggishness rather than an immediate loss of stability. Therefore, based on practical engineering considerations and to avoid unnecessary over-parameterization of the control law, a **robust passive fault-tolerant strategy** is adopted for the USVs. Any deviation or degradation in the USV actuators is mathematically incorporated into the bounded lumped disturbance term δ_i. The proposed fixed-time disturbance observer [Equations (27) and (28)] is specifically designed with high robustness to actively observe and reject this lumped term, which includes environmental forces and potential actuator variations. By combining active adaptive fault tolerance for the UAV with robust passive disturbance rejection for the USVs, the overall framework achieves comprehensive resilience. This asymmetric design is practically efficient and aligns well with the overall fault-tolerant theme of this heterogeneous cooperative control study.

where $\boldsymbol{M}_i \in \mathbb{R}^{3\times3}$ is the positive-definite inertia matrix that includes the added mass; $\boldsymbol{C}_i(\boldsymbol{v}_i) \in \mathbb{R}^{3\times3}$ is the Coriolis and centripetal matrix; and $\boldsymbol{D}_i \in \mathbb{R}^{3\times3}$ represents the linear hydrodynamic damping matrix. The vector $\boldsymbol{\tau}_i = [\tau_{iu}, \tau_{iv}, \tau_{ir}]^T$ denotes the control input, and $\boldsymbol{\delta}_i$ represents the lumped disturbances, including wind, wave, and current disturbances, as well as unmodeled dynamics. Considering the low-speed motion characteristics and geometric symmetry of the USV, the system matrices are specifically defined as follows:

$$\boldsymbol{M}_i = \mathrm{diag}\{m_{11}, m_{22}, m_{33}\} \tag{7}$$

$$\boldsymbol{D}_i = \mathrm{diag}\{d_{11}, d_{22}, d_{33}\} \tag{8}$$

$$\boldsymbol{C}_i(\boldsymbol{v}_i) = \begin{bmatrix} 0 & 0 & -m_{22}v_i \\ 0 & 0 & m_{11}u_i \\ m_{22}v_i & -m_{11}u_i & 0 \end{bmatrix} \tag{9}$$

2.2. UAV Model

Let the position of the UAV in the inertial coordinate system be $\boldsymbol{P} = [x, y, z]^T$, and its velocity be $\boldsymbol{v} = [\dot{x}, \dot{y}, \dot{z}]^T$. The dynamic model is described as follows:

$$\begin{bmatrix} \ddot{x} \\ \ddot{y} \\ \ddot{z} \end{bmatrix} = \frac{T}{m} \begin{bmatrix} \cos\phi \sin\theta \cos\psi + \sin\phi \sin\psi \\ \cos\phi \sin\theta \sin\psi - \sin\phi \cos\psi \\ \cos\theta \cos\phi \end{bmatrix} - \frac{1}{m} \begin{bmatrix} n_x \dot{x} \\ n_y \dot{y} \\ n_z \dot{z} \end{bmatrix} - \begin{bmatrix} 0 \\ 0 \\ g \end{bmatrix} \tag{10}$$

where x, y, z represents the UAV position in the inertial frame; m is the mass of the UAV; n_x, n_y, n_z are the aerodynamic damping coefficients; $\phi, \theta, and \psi$ denote the roll, pitch, and yaw angles, respectively; T is the total thrust; and g is the gravitational acceleration. To facilitate the design of the control loop, a virtual control input vector $\boldsymbol{U} = [U_x, U_y, U_z]^T$ is introduced. Since the UAV cannot directly generate horizontal thrust, the virtual control inputs calculated by the position controller must be converted into the desired thrust T and desired attitude angles ϕ_d and θ_d through attitude inversion. These quantities serve as reference inputs for the inner-loop attitude controller. The mapping relationship between the virtual control inputs and the physical quantities is defined as follows:

$$\begin{cases} U_x = (\cos\phi \sin\theta \cos\psi + \sin\phi \sin\psi) \dfrac{T}{m} \\ U_y = (\cos\phi \sin\theta \sin\psi - \sin\phi \cos\psi) \dfrac{T}{m} \\ U_z = \dfrac{T}{m} (\cos\theta \cos\phi) - g \end{cases} \tag{11}$$

This study adopts a hierarchical control architecture. The outer-loop position controller outputs the virtual control law $\boldsymbol{U}$. The desired attitude angles (ϕ_d, θ_d) are then obtained through inverse transformation to serve as references for the inner-loop attitude controller:

$$\phi_d = \arcsin\left(\frac{m(U_x \sin\psi - U_y \cos\psi)}{T}\right), \qquad \theta_d = \arctan\left(\frac{U_x \cos\psi + U_y \sin\psi}{U_z + g}\right) \tag{12}$$

Remark 2: The simplification in Equation (10) is based on the principle of time-scale separation. It is assumed that the bandwidth of the inner-loop attitude controller is significantly higher than that of the outer-loop position controller. According to Singular Perturbation Theory, when the inner-loop dynamics settle sufficiently rapidly (i.e., $\phi \to \phi_d$ and $\theta \to \theta_d$), the attitude dynamics can be viewed as the fast subsystem, allowing the position dynamics to be analyzed as the dominant slow subsystem. This is a standard assumption in UAV formation control.

Assuming that the inner-loop attitude controller possesses sufficiently high bandwidth to rapidly track the desired attitude (i.e., $\phi \approx \phi_d, \theta \approx \theta_d$), the dynamics of the position subsystem can be equivalently simplified as:

$$\begin{cases} \ddot{x} = U_x - \dfrac{n_x}{m} \dot{x} + d_x \\ \ddot{y} = U_y - \dfrac{n_y}{m} \dot{y} + d_y \\ \ddot{z} = U_z - \dfrac{n_z}{m} \dot{z} + d_z \end{cases} \tag{13}$$

where $d_x, d_y, and d_z$ represent lumped disturbance terms that incorporate unmodeled dynamics and external wind disturbances.

The UAV actuator fault model is described as follows:

$$u_k = \rho_k U_k + c_k, \qquad k \in \{x, y, z\} \tag{14}$$

where U_k is the ideal virtual control input calculated by the controller, and u_k is the actual effective control input applied to the system. The parameter $\rho_k \in (0, 1]$ represents the actuator efficiency factor, and c_k denotes the actuator bias fault.

Although the UAV thrust is generated through the coupling of the rotor system, a reduction in rotor speed generally results in a simultaneous decrease in control effectiveness along all three axes due to attitude coupling. This physical phenomenon suggests the existence of correlations among the efficiency factors of the three channels. However, the actuator bias term c_k may vary across channels due to sensor drift or mechanical asymmetry, requiring separate estimation through adaptive laws.

3. CONTROLLER DESIGN

3.1. Fixed-time controller design for USVs

To tackle the collaborative control problem of a heterogeneous UAV-USV system subject to external disturbances and actuator faults, a fixed-time adaptive distributed control strategy is proposed. For USV formation control, a leader-follower architecture is employed, consisting of one leader USV and three follower USVs. The trajectory of the leader USVs is assumed to be known or externally provided, and the follower USVs are tasked with maintaining a fixed relative geometric configuration with respect to the leader.

Definition 1 [40]**:** Consider a system described by $\dot{x} = f(x)$. The system is said to be fixed-time stable if there exists a bounded time $T_{\max} > 0$ such that, for any initial state $x(0)$, the system state satisfies $\lim_{t \to T(x(0))} x(t) = 0$, and the settling time satisfies $T(x(0)) \le T_{\max}$. Based on this theory, the fixed-time control law is designed as:

$$u = -k_1 \mathrm{sig}^{\alpha_1}(e) - k_2 \mathrm{sig}^{\alpha_2}(e) \tag{15}$$

where $\mathrm{sig}^{\alpha}(e) = |e|^{\alpha}\mathrm{sgn}(e)$, and the exponents satisfy:

$$\alpha_1 = 1 + \mu, \quad \alpha_2 = 1 - \mu, \quad 0 < \mu < 1 \tag{16}$$

To simplify the controller design, the position control (outer loop) and attitude control (inner loop) are decoupled. The backstepping method is adopted for the position loop design, assuming that the attitude control loop can rapidly and stably track the desired yaw angle. For control design, the planar position of the i-th USV is defined as $\boldsymbol{\eta}_i = [x_i, y_i]^T$ and its velocity is $\boldsymbol{v}_i = [u_i, v_i]^T$. The leader is indexed as $i = 1$, with position $\boldsymbol{\eta}_1 = [x_1, y_1]^T$ and desired trajectory $\boldsymbol{\eta}_d(t)$. To maintain a specific formation shape, the desired position of the i-th follower is defined as:

$$\boldsymbol{\eta}_{di} = \boldsymbol{\eta}_1 + \boldsymbol{\Delta}_i \tag{17}$$

where $\boldsymbol{\Delta}_i$ is the fixed position offset relative to the leader. Consequently, the formation tracking error is defined as:

$$\boldsymbol{e}_i = \boldsymbol{\eta}_i - \boldsymbol{\eta}_{di} = \boldsymbol{\eta}_i - (\boldsymbol{\eta}_1 + \boldsymbol{\Delta}_i) \tag{18}$$

For consistency, the position tracking error vector is also written as:

$$\boldsymbol{e}_{pi} = \boldsymbol{\eta}_i - \boldsymbol{\eta}_{di} \tag{19}$$

Taking the time derivative of $\boldsymbol{e}_{pi}$ and substituting the kinematic equation $\dot{\boldsymbol{\eta}}_i = \boldsymbol{R}(\psi_i)\boldsymbol{v}_i$, we obtain:

$$\dot{\boldsymbol{e}}_{pi} = \boldsymbol{R1}(\psi_i)\boldsymbol{v}_i - \dot{\boldsymbol{\eta}}_{di} \tag{20}$$

To ensure fixed-time convergence of the position error, a virtual control law $\boldsymbol{v}_{id}$ is designed as:

$$\boldsymbol{v}_{id} = \boldsymbol{R1}^T(\psi_i)\left[\dot{\boldsymbol{\eta}}_{di} - \boldsymbol{u}_{pi}\right] \tag{21}$$

where $\dot{\boldsymbol{\eta}}_{di} = \dot{\boldsymbol{\eta}}_1 + \dot{\boldsymbol{\Delta}}_i$ represents the derivative of the desired trajectory. The rotation matrix $\boldsymbol{R1}(\psi_i)$ is defined as:

$$\boldsymbol{R1}(\psi_i) = \begin{bmatrix} \cos\psi_i & -\sin\psi_i \\ \sin\psi_i & \cos\psi_i \end{bmatrix} \tag{22}$$

The auxiliary control term $\boldsymbol{u}_{pi}$ is designed with a fixed-time convergence structure:

$$\boldsymbol{u}_{pi} = k_{p1}\mathrm{sig}^{\alpha_1}(\boldsymbol{e}_{pi}) + k_{p2}\mathrm{sig}^{\alpha_2}(\boldsymbol{e}_{pi}) + \hat{\boldsymbol{d}}_{pi} \tag{23}$$

where $k_{p1}, k_{p2} > 0$ are control gains, and $\hat{\boldsymbol{d}}_{pi}$ is the estimated lumped disturbance in the position loop obtained online via an adaptive observer. The velocity tracking error is defined as:

$$\boldsymbol{e}_{vi} = [u_i, v_i]^T - \boldsymbol{v}_{id} \tag{24}$$

Considering planar motion, a reduced 2-degree-of-freedom (2-DOF) dynamic model is used. The actual control input τ_i is designed as:

$$\boldsymbol{\tau}_i = \boldsymbol{M}_i[\dot{\boldsymbol{v}}_{id} - \boldsymbol{u}_{vi}] + \boldsymbol{C}_i(\boldsymbol{v}_i)\boldsymbol{v}_i + \boldsymbol{D}_i\boldsymbol{v}_i \tag{25}$$

where $\boldsymbol{M}_i = \mathrm{diag}\{m_{11}, m_{22}\}$ is the inertia matrix, and $\boldsymbol{D}_i = \mathrm{diag}\{d_{11}, d_{22}\}$ is the damping matrix. The Coriolis matrix $\boldsymbol{C}_i(\boldsymbol{v}_i)$ captures the coupling effects of the USV motion. Similar to the position loop, the velocity stabilizing term $\boldsymbol{u}_{vi}$ adopts the fixed-time structure:

$$\boldsymbol{u}_{vi} = k_{v1}\mathrm{sig}^{\alpha_1}(\boldsymbol{e}_{vi}) + k_{v2}\mathrm{sig}^{\alpha_2}(\boldsymbol{e}_{vi}) + \hat{\boldsymbol{d}}_{vi} \tag{26}$$

where $\hat{\boldsymbol{d}}_{vi}$ represents the estimated disturbance in the velocity loop. To address actuator faults and external environmental disturbances, a dual-layer adaptive disturbance observer is designed. This observer ensures that disturbance estimation errors converge to zero within a fixed time, providing accurate compensation to the controller. The dynamics of the position loop disturbance observer is given by:

$$\dot{\hat{\boldsymbol{d}}}_{pi} = \gamma_{p1}\mathrm{sig}^{\beta_1}(\boldsymbol{e}_{pi}) + \gamma_{p2}\mathrm{sig}^{\beta_2}(\boldsymbol{e}_{pi}) \tag{27}$$

The dynamics of the velocity loop disturbance observer is given by:

$$\dot{\hat{\boldsymbol{d}}}_{vi} = \gamma_{v1}\mathrm{sig}^{\beta_1}(\boldsymbol{e}_{vi}) + \gamma_{v2}\mathrm{sig}^{\beta_2}(\boldsymbol{e}_{vi}) \tag{28}$$

where $\gamma_{p1}, \gamma_{p2}, \gamma_{v1}, and \gamma_{v2}$ are positive observer gains. To satisfy the fixed-time stability condition, the power parameters are selected as:

$$\beta_1 = 1 + \frac{\mu}{2}, \qquad \beta_2 = 1 - \frac{\mu}{2} \tag{29}$$

This observer structure guarantees that the estimation errors for lumped disturbances (including those caused by unmodeled dynamics and wind/wave forces) converge to the origin in a fixed time, independent of initial estimation errors.

3.2. Prescribed performance controller design for UAV

To achieve the desired tracking performance, the overall control architecture proposed in this paper is shown in Figure 2. It mainly consists of a trajectory tracking controller, a fault-tolerant mechanism, and a disturbance observer. PPC is an advanced control strategy designed to precisely regulate both transient and steady-state tracking performance. Its fundamental idea involves designing time-varying performance functions to establish strict boundaries for the error convergence process, thereby ensuring that overshoot, convergence rate, and steady-state precision satisfy predefined requirements.

In the proposed framework, the UAV tracks the geometric center of the USV formation as its target. Let the UAV position in the inertial frame be $\boldsymbol{\eta}_a = [x_a, y_a, z_a]^T$, and the formation center position be $\boldsymbol{\eta}_c = [x_c, y_c, 0]^T$. The formation tracking error, denoted as $\boldsymbol{e}_a$, is defined as:

$$\boldsymbol{e}_a = \begin{bmatrix} e_x \\ e_y \\ e_z \end{bmatrix} = \begin{bmatrix} x_a - x_c - \Delta x_d \\ y_a - y_c - \Delta y_d \\ z_a - H_d \end{bmatrix} \tag{30}$$

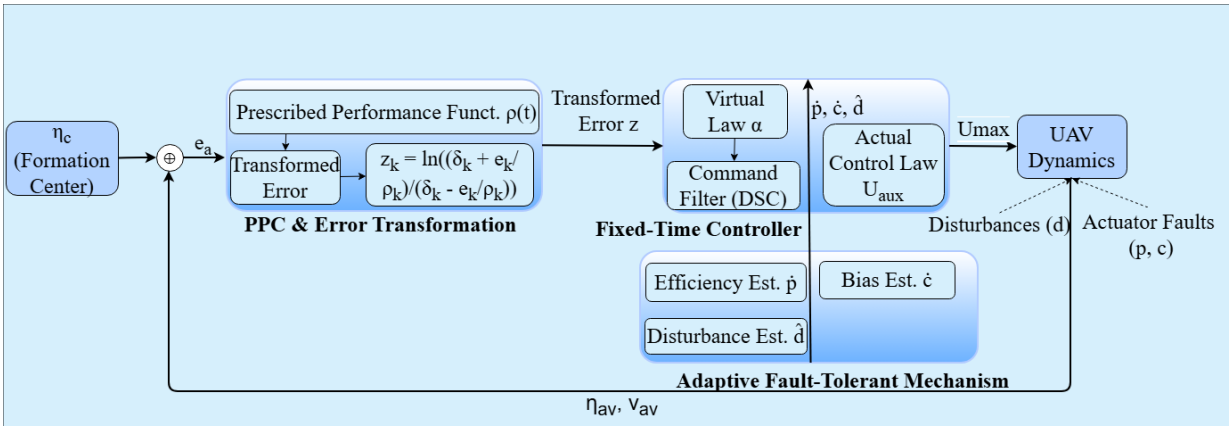

Figure 2. Block diagram of the proposed fixed-time prescribed performance fault-tolerant control strategy for the UAV subsystem. The architecture integrates error transformation, command filtering, and adaptive compensation to handle safety constraints and actuator faults. UAV: Unmanned aerial vehicle; PPC: prescribed performance control; DSC: dynamic surface control.

where Δx_d and Δy_d represent the desired horizontal offsets relative to the formation center, and H_d denotes the desired flight altitude.

Accordingly, the error dynamics are given by:

$$\dot{\boldsymbol{e}}_a = \begin{bmatrix} \dot{e}_x \\ \dot{e}_y \\ \dot{e}_z \end{bmatrix} = \begin{bmatrix} v_{ax} - \dot{x}_c \\ v_{ay} - \dot{y}_c \\ v_{az} \end{bmatrix} \tag{31}$$

where $[v_{ax}, v_{ay}, v_{az}]^T$ is the UAV velocity vector.

To achieve fixed-time convergence of tracking errors, a performance function $p_k(t)$ is designed for each channel $k \in \{x, y, z\}$. It defines the allowable evolution boundary of the tracking error:

$$p_k(t) = (p_{0k} - p_{\infty k})\varphi(t) + p_{\infty k}, \qquad k \in \{x, y, z\} \tag{32}$$

where p_{0k} and $p_{\infty k}$ represent the initial and the final (steady-state) values of the performance function, respectively, satisfying the condition $0 < p_{\infty k} < p_{0k}$. The function $\varphi(t)$ is a specially designed polynomial decay function that ensures convergence within a fixed time T_f:

$$\varphi(t) = \begin{cases} \dfrac{(T_f - t)^2}{T_f^2}, & 0 \le t \le T_f \\ 0, & t > T_f \end{cases} \tag{33}$$

Direct controller design based on the constrained error $\boldsymbol{e}_a$ would result in complex nonlinear inequality constraints. Therefore, an *evolution path* and an *error transformation function* are introduced to convert the constrained problem into an unconstrained one.

The evolution path $Y_k(t)$ is introduced as a "transitional trajectory" to guide the smooth convergence of the error. Its primary function is to eliminate initial error jumps (especially when the initial error is large) and to ensure smoothness of the control input.

The evolution path is designed as:

$$Y_k(t) = \begin{cases} \dfrac{e_{0k}}{T_c^n}(T_c - t)^n, & 0 \le t \le T_c \\ 0, & t > T_c \end{cases} \tag{34}$$

The introduction of $Y_k(t)$ serves a critical role in handling initial errors. Unlike traditional PPC, where the initial error must be strictly within bounds, the evolution path ensures that $e(0) - Y(0) = 0$, eliminating the risk of "term explosion" in the control input at $t = 0$ due to large initial deviations. The parameter $n \geq 2$ is selected to ensure sufficient smoothness of the evolution path (i.e., its first- and second-order derivatives exist and are continuous over $t = 0$ and $t = T_c$).

Here, T_c is the desired convergence time (matched with the performance function); $n \geq 2$ is a smoothness parameter; and e_{0k} is the initial error, ensuring that the path starts exactly from the initial error value.

Define the deviation between the actual error and the ideal evolution path as:

$$\varepsilon_k = e_k - Y_k \tag{35}$$

where ε_k satisfies the constraint $-\delta_k p_k(t) < \varepsilon_k < \delta_k p_k(t)$, with $0 < \delta_k \leq 1$. To transform the constrained variable ε_k into an unconstrained one, the following nonlinear logarithmic transformation function is introduced:

$$z_k = \frac{1}{2} \ln \left(\frac{\delta_k + \frac{\varepsilon_k}{p_k(t)}}{\delta_k - \frac{\varepsilon_k}{p_k(t)}} \right) \tag{36}$$

The logarithmic function transforms the constrained error ε_k defined in the domain $(-\delta_k p_k, \delta_k p_k)$ into an unconstrained variable $z_k \in (-\infty, +\infty)$. This transformation allows the subsequent controller design to proceed without explicitly handling inequality constraints.

Here, z_k represents the transformed unconstrained error. When $\varepsilon_k \in (-\delta_k p_k(t), \delta_k p_k(t))$, there exists a one-to-one mapping between z_k and ε_k. Furthermore, as $\varepsilon_k \to \pm\delta_k p_k(t)$, it follows that $z_k \to \pm\infty$. This property inherently prevents the constraints from being violated.

Taking the time derivative of z_k, we obtain:

$$\dot{z}_k = r_k(t) \left(\dot{\varepsilon}_k - \frac{\varepsilon_k \dot{p}_k(t)}{p_k(t)} \right) \tag{37}$$

where the intermediate term $r_k(t)$ is given by:

$$r_k(t) = \frac{\partial z_k}{\partial(\varepsilon_k / p_k)} \cdot \frac{1}{p_k(t)} = \frac{\delta_k}{p_k(t) \left(\delta_k^2 - \left(\frac{\varepsilon_k}{p_k(t)} \right)^2 \right)} \tag{38}$$

This transformed dynamics $\dot{z}_k$ will be used in the subsequent controller design to ensure system stability.

Based on the dynamics of the transformed error z, a hierarchical control strategy consisting of "virtual control" and "actual control" is adopted. To avoid the "explosion of terms" inherent in traditional backstepping methods when calculating high-order derivatives, a first-order command filter is introduced to achieve smooth and stable convergence.

First, the dynamics of the transformed error system can be expressed in vector form as:

$$\dot{\boldsymbol{z}} = \boldsymbol{\Psi}(\dot{\boldsymbol{\varepsilon}} - \boldsymbol{\Pi}) \tag{39}$$

where $\dot{\boldsymbol{\varepsilon}} = \dot{\boldsymbol{e}}_a - \dot{\boldsymbol{Y}}$. The vector $\boldsymbol{\Pi}$ and the Jacobian matrix $\boldsymbol{\Psi}$ are defined as:

$$\boldsymbol{\Pi} = \begin{bmatrix} \frac{\varepsilon_x \dot{p}_x}{p_x} \\ \frac{\varepsilon_y \dot{p}_y}{p_y} \\ \frac{\varepsilon_z \dot{p}_z}{p_z} \end{bmatrix}, \quad \boldsymbol{\Psi} = \mathrm{diag}\{r_x, r_y, r_z\} \tag{40}$$

Virtual Control Law Design: The virtual control law $\boldsymbol{\alpha}$ serves as the desired velocity reference. To ensure the stability of the position loop, $\boldsymbol{\alpha}$ is designed as:

$$\boldsymbol{\alpha} = -\boldsymbol{\Psi}^{-1}\boldsymbol{K}_1 z + \dot{\boldsymbol{Y}} + \boldsymbol{\Pi} + \dot{\boldsymbol{\eta}}_c \tag{41}$$

where $\boldsymbol{K}_1$ is a positive definite gain matrix, and $\dot{\boldsymbol{\eta}}_c = [\dot{x}_c, \dot{y}_c, 0]^T$ represents the velocity of the formation center. Note that the virtual control law α is designed directly in the inertial frame to maintain consistency with the position error z, thus simplifying the backstepping control law without loss of generality.

Command Filter Design: Since the virtual control law $\boldsymbol{\alpha}$ involves high-order derivatives of the error, directly using it for differentiation would cause severe fluctuations in the control input. Therefore, a first-order filter is introduced to smooth the virtual control signal:

$$\tau_f \dot{\boldsymbol{\alpha}}_f + \boldsymbol{\alpha}_f = \boldsymbol{\alpha}, \qquad \boldsymbol{\alpha}_f(0) = \boldsymbol{\alpha}(0) \tag{42}$$

where τ_f is the filter time constant, and $\boldsymbol{\alpha}_f$ denotes the smoothed desired velocity. Accordingly, the filter error $\boldsymbol{y}$ and its dynamics are defined as follows:

$$\boldsymbol{y} = \boldsymbol{\alpha}_f - \boldsymbol{\alpha}, \qquad \dot{\boldsymbol{y}} = -\frac{1}{\tau_f}\boldsymbol{y} - \dot{\boldsymbol{\alpha}} \tag{43}$$

Actual Control Law Design: Define the actual velocity tracking error as:

$$\boldsymbol{s} = \boldsymbol{v}_a - \boldsymbol{\alpha}_f \tag{44}$$

Based on the equation of UAV dynamics $m_a \dot{\boldsymbol{v}}_a = \boldsymbol{\rho}\boldsymbol{U}_a + \boldsymbol{c} + \boldsymbol{d}_a$, and considering compensation for actuator faults and disturbances, the actual control law $\boldsymbol{U}_a$ is designed as:

$$\boldsymbol{U}_a = \hat{\boldsymbol{\rho}}^{-1}\left[m_a(-\boldsymbol{K}_2\boldsymbol{s} + \dot{\boldsymbol{\alpha}}_f) - \hat{\boldsymbol{c}} - \hat{\boldsymbol{d}}_a - \boldsymbol{\Psi}^T z\right] \tag{45}$$

where $\boldsymbol{K}_2$ is a positive definite gain matrix for the velocity loop. $\hat{\boldsymbol{\rho}}$, $\hat{\boldsymbol{c}}$, and $\hat{\boldsymbol{d}}_a$ are the adaptive estimates of the actuator efficiency matrix, bias fault, and lumped disturbances, respectively. The term $-\boldsymbol{\Psi}^T z$ is introduced to eliminate the coupling effects arising from the coordinate transformation during the stability analysis.

3.3. Adaptive update laws design

To estimate the unknown parameters $\boldsymbol{\rho}$, $\boldsymbol{c}$, and $\boldsymbol{d}_a$ online, adaptive update laws are designed based on Lyapunov stability theory.

First, define the parameter estimation errors:

$$\tilde{\boldsymbol{\rho}} = \boldsymbol{\rho} - \hat{\boldsymbol{\rho}}, \qquad \tilde{\boldsymbol{c}} = \boldsymbol{c} - \hat{\boldsymbol{c}}, \qquad \tilde{\boldsymbol{d}}_a = \boldsymbol{d}_a - \hat{\boldsymbol{d}}_a \tag{46}$$

Consider the following Lyapunov candidate terms for parameter adaptation:

$$V_\rho = \frac{1}{2}\mathrm{tr}(\tilde{\boldsymbol{\rho}}^T\boldsymbol{\Gamma}_\rho^{-1}\tilde{\boldsymbol{\rho}}), \qquad V_c = \frac{1}{2}\tilde{\boldsymbol{c}}^T\boldsymbol{\Gamma}_c^{-1}\tilde{\boldsymbol{c}}, \qquad V_d = \frac{1}{2}\tilde{\boldsymbol{d}}_a^T\boldsymbol{\Gamma}_d^{-1}\tilde{\boldsymbol{d}}_a \tag{47}$$

where $\boldsymbol{\Gamma}_\rho, \boldsymbol{\Gamma}_c, \boldsymbol{\Gamma}_d$ are positive definite symmetric adaptive gain matrices.

Taking the time derivative of V_ρ yields $\dot{V}_\rho = \mathrm{tr}(\tilde{\boldsymbol{\rho}}^T\boldsymbol{\Gamma}_\rho^{-1}\dot{\tilde{\boldsymbol{\rho}}}) = -\mathrm{tr}(\tilde{\boldsymbol{\rho}}^T\boldsymbol{\Gamma}_\rho^{-1}\dot{\hat{\boldsymbol{\rho}}})$. To eliminate the cross-coupling terms appearing in the time derivative of the velocity error subsystem (specifically the term $\boldsymbol{s}^T\tilde{\boldsymbol{\rho}}\boldsymbol{U}_a$), and to incorporate σ-modification for preventing parameter drift, the adaptive update laws are designed as follows:

$$\dot{\hat{\boldsymbol{\rho}}} = \boldsymbol{\Gamma}_\rho \boldsymbol{s}\boldsymbol{U}_a^T - \boldsymbol{\Sigma}_\rho\hat{\boldsymbol{\rho}} \tag{48}$$

$$\dot{\hat{\boldsymbol{c}}} = \boldsymbol{\Gamma}_c \boldsymbol{s} - \boldsymbol{\Sigma}_c\hat{\boldsymbol{c}} \tag{49}$$

$$\dot{\hat{\boldsymbol{d}}}_a = \boldsymbol{\Gamma}_d \boldsymbol{s} - \boldsymbol{\Sigma}_d\hat{\boldsymbol{d}}_a \tag{50}$$

where $\boldsymbol{\Sigma}_\rho, \boldsymbol{\Sigma}_c, and \boldsymbol{\Sigma}_d$ are positive design parameters for robust modification terms. These laws ensure that the estimates converge to a bounded region near their true values.

4. STABILITY ANALYSIS

4.1. Fixed-time stability proof for USV formation

Construct the following composite Lyapunov candidate function:

$$V = \frac{1}{2}\sum_{i=2}^{N}\left(e_{pi}^{T}e_{pi} + e_{vi}^{T}M_i e_{vi} + \tilde{d}_{pi}^{T}\Gamma_p^{-1}\tilde{d}_{pi} + \tilde{d}_{vi}^{T}\Gamma_v^{-1}\tilde{d}_{vi}\right) \tag{51}$$

where $\tilde{d} = d - \hat{d}$ represents the disturbance estimation error, $\Gamma_p, \Gamma_v > 0$ are positive definite diagonal gain matrices, and M_i is the positive definite symmetric inertia matrix of the i-th USV.

Taking the time derivative of the Lyapunov function V yields:

$$\dot{V} = \sum_{i=2}^{N}\left(e_{pi}^{T}\dot{e}_{pi} + e_{vi}^{T}M_i\dot{e}_{vi} + \tilde{d}_{pi}^{T}\Gamma_p^{-1}\dot{\tilde{d}}_{pi} + \tilde{d}_{vi}^{T}\Gamma_v^{-1}\dot{\tilde{d}}_{vi}\right) \tag{52}$$

Step 1: Position Loop Dynamics. Substituting the kinematic equation and the virtual control definition, the derivative of the position error is derived as:

$$\dot{e}_{pi} = -\dot{\eta}_{di} + R1(\psi_i)v_i \tag{53}$$

Recalling that $v_i = e_{vi} + v_{id}$, and expanding the virtual control law, we obtain:

$$\dot{e}_{pi} = R1(\psi_i)e_{vi} - u_{pi} + d_{pi} \tag{54}$$

where u_{pi} contains the stabilizing feedback term and the compensation of the disturbance. Consequently, the first term in $\dot{V}$ becomes:

$$e_{pi}^{T}\dot{e}_{pi} = e_{pi}^{T}\left[R1(\psi_i)e_{vi} - u_{pi} + d_{pi}\right] \tag{55}$$

Step 2: Velocity Loop Dynamics. Substituting the USV dynamics and the actual control law τ_i into the second term, it is crucial to note that, based on the backstepping design principle, the actual control law implicitly includes a compensation term $-R1^{T}(\psi_i)e_{pi}$ to eliminate the coupling effect from the position loop. The closed-loop dynamics of the velocity error can be simplified as:

$$M_i\dot{e}_{vi} = -M_i u_{vi} + \tilde{d}_{vi} - R1^{T}(\psi_i)e_{pi} \tag{56}$$

Thus, the second term in $\dot{V}$ becomes:

$$e_{vi}^{T}M_i\dot{e}_{vi} = -e_{vi}^{T}M_i u_{vi} + e_{vi}^{T}\tilde{d}_{vi} - e_{vi}^{T}R1^{T}(\psi_i)e_{pi} \tag{57}$$

From the above equations, it can be observed that the coupling term $e_{pi}^{T}R1(\psi_i)e_{vi}$ in the position loop exactly cancels with the term $-e_{vi}^{T}R1^{T}(\psi_i)e_{pi}$ in the velocity loop.

Step 3: Disturbance Estimation Error. Assuming that the external disturbance varies slowly relative to the observer dynamics, i.e., $\dot{d} \approx 0$, we obtain $\dot{\tilde{d}} = -\dot{\hat{d}}$. Substituting the observer update laws:

$$\dot{\hat{d}}_{pi} = \Gamma_p\left(\mathrm{sig}^{\beta_1}(e_{pi}) + \mathrm{sig}^{\beta_2}(e_{pi})\right) \tag{58}$$

$$\dot{\hat{d}}_{vi} = \Gamma_v\left(\mathrm{sig}^{\beta_1}(e_{vi}) + \mathrm{sig}^{\beta_2}(e_{vi})\right) \tag{59}$$

These observer dynamics are designed to stabilize the estimation error subsystem within a fixed time.

Substituting all terms back into $\dot{V}$, and using the fixed-time stability properties of $\boldsymbol{u}_{pi}$ and $\boldsymbol{u}_{vi}$ (which contain terms such as $-k_1\mathrm{sig}^{\alpha_1}(\boldsymbol{e})-k_2\mathrm{sig}^{\alpha_2}(\boldsymbol{e})$), it can be proven that the time derivative of the Lyapunov function satisfies the following fixed-time stability condition:

$$\dot{V} \le -\mu_1 V^{\frac{1+\mu}{2}} - \mu_2 V^{\frac{1-\mu}{2}} + C \tag{60}$$

Remark 3: Since the residual term C satisfies $C > 0$, the system achieves practical fixed-time stability (P-FTS) rather than exact asymptotic convergence to zero. The tracking error converges to a neighborhood of the origin Ω_e within a bounded settling time T_{max}. The upper bound of the settling time is estimated as:

$$T_{max} \le \frac{1}{\mu_1\theta\left(1-\frac{1+\mu}{2}\right)} + \frac{1}{\mu_2\theta\left(\frac{1-\mu}{2}-1\right)}$$

where $0 < \theta < 1$ is a scalar parameter. The convergence region is bounded by the set where the stabilizing terms dominate the residual term C.

Here, $\mu_1, \mu_2 > 0$, and C is a small residual constant. This inequality guarantees that the tracking errors $\boldsymbol{e}_{pi}$ and $\boldsymbol{e}_{vi}$ converge to a small neighborhood of the origin within a fixed time $T_{\max}$, independent of the initial states.

4.2. Stability proof for the UAV subsystem

Construct the following composite Lyapunov candidate function:

$$V_{UAV} = V_1 + V_2 + V_3 + V_4 \tag{61}$$

where the components are defined as:

$$V_1 = \frac{1}{2}z^T z \quad \text{(Transformed error energy)} \tag{62}$$

$$V_2 = \frac{1}{2}s^T m_a s \quad \text{(Velocity tracking error energy)} \tag{63}$$

$$V_3 = \frac{1}{2}y^T y \quad \text{(Filter error energy)} \tag{64}$$

$$V_4 = \frac{1}{2}\mathrm{tr}(\tilde{\rho}^T\Gamma_\rho^{-1}\tilde{\rho}) + \frac{1}{2}\tilde{c}^T\Gamma_c^{-1}\tilde{c} + \frac{1}{2}\tilde{d}_a^T\Gamma_d^{-1}\tilde{d}_a \quad \text{(Estimation error energy)} \tag{65}$$

4.2.1. Time derivative and convergence analysis

Lemma 2 (Boundedness of Transformation Terms): Assume that the performance function $p_k(t)$ satisfies $p_k(t) \ge p_{\infty k} > 0$ and that its time derivatives are bounded by design. As long as the error remains within the prescribed limits (which is guaranteed by the logarithmic mapping property of z_k), the term $1/p_k(t)$ is bounded. Consequently, the Jacobian matrix

$$\Psi = \mathrm{diag}\{r_x, r_y, r_z\}$$

and its time derivative $\dot{\Psi}$ remain bounded throughout the operation. Let

$$\|\Psi\| \le \Psi_M.$$

Taking the time derivative of V_1 and substituting the transformed error dynamics $\dot{z} = \boldsymbol{\Psi}(\dot{\boldsymbol{e}}_a - \dot{\boldsymbol{Y}} - \boldsymbol{\Pi})$, yields:

$$\dot{V}_1 = z^T\dot{z} = z^T\boldsymbol{\Psi}(\dot{\boldsymbol{e}}_a - \dot{\boldsymbol{Y}} - \boldsymbol{\Pi}) \tag{66}$$

Substituting the formation error derivative $\dot{\boldsymbol{e}}_a = \boldsymbol{R}(\psi)\boldsymbol{v}_a - \dot{\boldsymbol{\eta}}_c$, where $\boldsymbol{R}(\psi)$ projects the body velocity to the inertial frame, gives:

$$\dot{V}_1 = z^T\boldsymbol{\Psi}(\boldsymbol{v}_a - \dot{\boldsymbol{\eta}}_c - \dot{\boldsymbol{Y}} - \boldsymbol{\Pi}) \tag{67}$$

Using the velocity definition $\boldsymbol{v}_a = \boldsymbol{s} + \boldsymbol{y} + \boldsymbol{\alpha}$, the above expression becomes:

$$\dot{V}_1 = z^T\boldsymbol{\Psi}[(\boldsymbol{s} + \boldsymbol{y} + \boldsymbol{\alpha}) - \dot{\boldsymbol{\eta}}_c - \dot{\boldsymbol{Y}} - \boldsymbol{\Pi}] \tag{68}$$

Substituting the designed virtual control law $\alpha = -\Psi^{-1}K_1 z + \dot{Y} + \Pi + \dot{\eta}_c$, yields:

$$\begin{aligned}\dot{V}_1 &= z^T\Psi(s+y) + z^T\Psi[\alpha - (\dot{Y} + \Pi + \dot{\eta}_c)] \\ &= z^T\Psi(s+y) + z^T\Psi[-\Psi^{-1}K_1 z] \\ &= -z^T K_1 z + z^T\Psi s + z^T\Psi y\end{aligned} \tag{69}$$

Considering the UAV dynamics $m_a\dot{v}_a = \rho U_a + c + d_a$, the derivative of V_2 is:

$$\dot{V}_2 = s^T m_a\dot{s} = s^T(m_a\dot{v}_a - m_a\dot{\alpha}_f) = s^T(\rho U_a + c + d_a - m_a\dot{\alpha}_f) \tag{70}$$

The parameters are decomposed into their true values and estimates (e.g., $\rho = \hat{\rho} + \tilde{\rho}$):

$$\dot{V}_2 = s^T(\hat{\rho}U_a + \hat{c} + \hat{d}_a - m_a\dot{\alpha}_f) + s^T(\tilde{\rho}U_a + \tilde{c} + \tilde{d}_a) \tag{71}$$

Substituting the actual control law $U_a = \hat{\rho}^{-1}[m_a(-K_2 s + \dot{\alpha}_f) - \hat{c} - \hat{d}_a - \Psi^T z]$, yields:

$$\begin{aligned}\dot{V}_2 &= s^T[m_a(-K_2 s + \dot{\alpha}_f) - \hat{\rho}U_a - \hat{c} - \hat{d}_a - \Psi^T z + \hat{\rho}U_a + \hat{c} + \hat{d}_a - m_a\dot{\alpha}_f] \\ &\quad + s^T(\tilde{\rho}U_a + \tilde{c} + \tilde{d}_a) \\ &= -s^T m_a K_2 s - s^T\Psi^T z + s^T\tilde{\rho}U_a + s^T\tilde{c} + s^T\tilde{d}_a \\ &= -s^T m_a K_2 s - z^T\Psi s + s^T\tilde{\rho}U_a + s^T\tilde{c} + s^T\tilde{d}_a\end{aligned} \tag{72}$$

Using the filter dynamics $\dot{y} = -y/\tau_f - \dot{\alpha}$, the derivative of V_3 is given by:

$$\dot{V}_3 = y^T\dot{y} = -\frac{y^T y}{\tau_f} - y^T\dot{\alpha} \tag{73}$$

Applying Young's inequality, $-y^T\dot{\alpha} \le \frac{1}{2}y^T y + \frac{1}{2}\|\dot{\alpha}\|^2$, where $\dot{\alpha}$ is assumed to be bounded.

For V_4, taking the derivative yields:

$$\dot{V}_4 = -\mathrm{tr}(\tilde{\rho}^T\Gamma_\rho^{-1}\dot{\hat{\rho}}) - \tilde{c}^T\Gamma_c^{-1}\dot{\hat{c}} - \tilde{d}_a^T\Gamma_d^{-1}\dot{\hat{d}}_a \tag{74}$$

Combining all terms yields:

$$\dot{V}_{UAV} = -z^T K_1 z - s^T m_a K_2 s - \frac{y^T y}{\tau_f} + z^T\Psi y - y^T\dot{\alpha} + \text{Adaptive Terms} \tag{75}$$

Substituting the adaptive update laws with σ-modification, the "Adaptive Terms" become:

$$\text{Adaptive Terms} = \mathrm{tr}(\tilde{\rho}^T\Sigma_\rho\hat{\rho}) + \tilde{c}^T\Sigma_c\hat{c} + \tilde{d}_a^T\Sigma_d\hat{d}_a \tag{76}$$

Using the inequality $\tilde{\theta}^T\hat{\theta} = \tilde{\theta}^T(\theta - \tilde{\theta}) \le -\frac{1}{2}\|\tilde{\theta}\|^2 + \frac{1}{2}\|\theta\|^2$, the adaptive terms contribute to the negative definiteness and a bounded constant.

Finally, for the cross term $z^T\Psi y$, applying Young's inequality gives:

$$z^T\Psi y \le \frac{1}{2}\|z\|^2 + \frac{1}{2}\|\Psi_M\|^2\|y\|^2 \tag{77}$$

Since Ψ is bounded by the design of the performance function, the overall derivative satisfies:

$$\dot{V}_{UAV} \le -CV_{UAV} + D \tag{78}$$

where $C > 0$ and D is a small positive constant. This shows that all error signals in the UAV subsystem are uniformly ultimately bounded (UUB) and converge to a small neighborhood of the origin.

Remark 4 (Convergence Time Analysis): The Lyapunov analysis in Equation (75) proves that the transformed error z_k is UUB. However, due to the inverse logarithmic mapping defined in Equation (33), the boundedness of z_k strictly implies that the normalized error $\xi_k = \varepsilon_k/p_k(t)$ remains within $(-1, 1)$. Consequently, the actual

tracking error $\varepsilon_k(t)$ is strictly restricted within the envelope $(-\delta_k p_k(t), \delta_k p_k(t))$. Since the performance function $p_k(t)$ is designed to decay to $p_{\infty k}$ at a pre-specified fixed time T_f [as shown in Equation (30)], the tracking error ε_k is mathematically guaranteed to converge to the small region $\{e : |e| < \delta_k p_{\infty k}\}$ by time T_f. Thus, the fixed-time convergence property is enforced through the PPC mechanism.

5. SIMULATION AND COMPARATIVE ANALYSIS

To verify the effectiveness and robustness of the proposed heterogeneous fixed-time prescribed performance formation control strategy, numerical simulations are conducted. To rigorously validate the necessity of each module (PPC and Adaptive Observer) in the UAV subsystem, we conducted a comparative study involving three distinct cases.

- **Case 1 (Proposed method):** The complete algorithm, which incorporates fixed-time PPC, evolution path, and an adaptive fault-tolerant mechanism.

- **Case 2 (Without Observer):** An ablation study in which fault compensation is disabled (i.e., $\hat{\rho}_k \equiv 1, \hat{c}_k \equiv 0, \hat{d}_k \equiv 0$).

- **Case 3 (Without PPC):** A comparative study using a standard fixed-time sliding mode controller without prescribed performance constraints.

5.1. Simulation setup

The simulations are performed using MATLAB with a fixed time step of $dt = 0.005$ s over a duration of $t = 30$ s. The heterogeneous system comprises $N = 4$ USVs and a single UAV.

5.1.1. Trajectory and physical parameters

The USV formation is tasked with tracking a virtual leader moving along a circular trajectory defined by $x_r = 5\cos(0.1t)$ and $y_r = 5\sin(0.1t)$, while the UAV is required to track the geometric center of the USV formation while maintaining a desired relative altitude of $H_d = 5$ m. The physical parameters of the USVs are set as: the mass matrix $\boldsymbol{M}_i = \text{diag}\{20, 15, 5\}$ and the damping matrix $\boldsymbol{D}_i = \text{diag}\{2, 1.5, 0.8\}$. The UAV mass is $m_a = 1$ kg with the gravitational acceleration $g = 9.8\text{m/s}^2$.

5.1.2. Topology and initial states

The formation topology is defined by the relative position offsets Λ_i with respect to the leader: USV 1 (Leader) is located at $[0, 0]^{\mathrm{T}}$, USV 2 at $[1.5, 0]^{\mathrm{T}}$, USV 3 at $[-1.5, 0]^{\mathrm{T}}$, and USV 4 at $[0, 1]^{\mathrm{T}}$. The initial states are set as follows:

- USVs: $\boldsymbol{\eta}_1 = [0, 0, 0]^{\mathrm{T}}$ with an initial surge velocity $u_1 = 0.5$ m/s, $\boldsymbol{\eta}_2 = [1, 1, 0]^{\mathrm{T}}$, $\boldsymbol{\eta}_3 = [0, 2, 0]^{\mathrm{T}}$, and $\boldsymbol{\eta}_4 = [2, 2, 0]^{\mathrm{T}}$.

- UAV: Initial position $\boldsymbol{P}_0 = [2, 2, 5.0]^{\mathrm{T}}$ and initial vertical velocity $v_{z0} = -0.5$ m/s.

5.1.3. Control and fault parameters

To validate fixed-time convergence and fault tolerance, the control parameters of the **Proposed** method are selected as:

- **Fixed-Time Parameters:** Power parameter $\mu = 0.5$ (yielding $\alpha_1 = 1.5, \alpha_2 = 0.5$).

- **USV Gains:** Position loop gains $k_{p1} = 2, k_{p2} = 1.5$; Velocity loop gains $k_{v1} = 3, k_{v2} = 2$; Observer gains $\gamma_{p1} = 1, \gamma_{v1} = 1.5$.

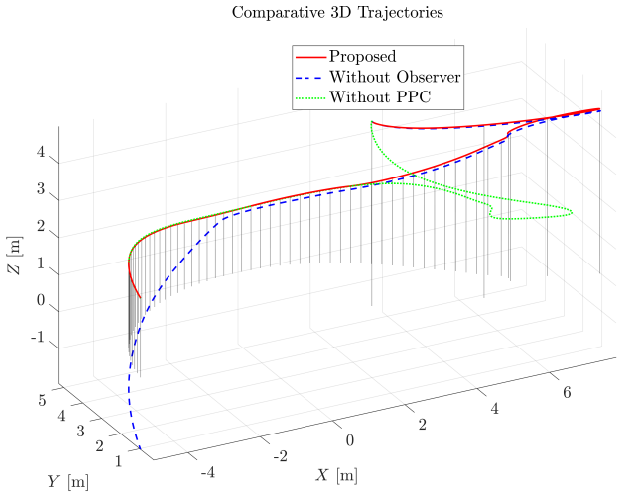

Figure 3. Comparative 3D trajectories. The Proposed method (red) tracks the reference smoothly, while the Without Observer case (blue) suffers from altitude deviation. PPC: Prescribed performance control.

• **UAV PPC Parameters:** The performance function parameters are set with initial boundaries $p_{0k} = 1.5|e_k(0)|$ and steady-state error limits $\boldsymbol{p}_\infty = [0.05, 0.05, 0.1]^{\mathrm{T}}$. The smoothness parameter of the evolution path is $n = 2$, and the constraint parameter is $\delta_k = 1$.

• **UAV Controller Gains:** Virtual control gain $\boldsymbol{K}_1 = \mathrm{diag}\{4, 4, 2.5\}$, actual control gain $\boldsymbol{K}_2 = \mathrm{diag}\{8, 8, 4.0\}$, and filter time constant $\tau_f = 0.1$.

Furthermore, to test the adaptive compensation mechanism under different fault scenarios (Case 1 and Case 2), actuator faults are introduced into the UAV with an efficiency factor $\boldsymbol{\rho} = \mathrm{diag}\{0.9, 0.9, 0.9\}$ (representing a 10% thrust loss) and bias faults $\boldsymbol{c} = [0.05, 0.05, 0.05]^{\mathrm{T}}$.

5.2. Comparative analysis of UAV trajectory

Figure 3 presents a comparison of the 3D trajectories of the heterogeneous system. The **Proposed** method (red solid line) follows the spiral ascending track easily and sustains the formation structure perfectly. In contrast, the **Without PPC** case (green dotted line) exhibits pronounced oscillations in the initial stage due to the absence of transient constraints. Most importantly, in the **Without Observer** case (blue dashed line), the UAV suffers from a severe altitude drop (Z-axis). This is because the 10% thrust loss ($\rho = 0.9$) remains uncompensated, preventing the system from generating sufficient lift to counteract gravity, confirming the necessity of the "fault-tolerant" nature of our design. It is crucial to clarify that a 10% efficiency loss is not an exaggerated fault setting. Because rotary-wing UAVs rely entirely on actuator-generated thrust to counteract gravity, their steady-state thrust margin is strictly limited. An uncompensated 10% loss in total lifting capability directly disrupts the delicate balance required for hovering and altitude tracking, inevitably leading to the pronounced altitude deviation observed. This physical constraint underscores the critical need for the proposed adaptive observer.

5.3. Comparative error analysis of UAV

Figure 4 provides a more detailed understanding of control quality. **Transient Smoothness:** While the **Without PPC** case (green) stays within the boundaries in this setup, it exhibits pronounced jitter and non-smooth "sharp turns" in the X and Y channels during the first 2 s. In contrast, the **Proposed** method (red) follows the Ideal Evolution Path (grey dots) with superior smoothness. **Boundary Enforcement:** The PPC boundaries (black dashed lines) strictly envelope the red trajectory. **Critical Failure Analysis:** In the Z-error subplot, the **Without**

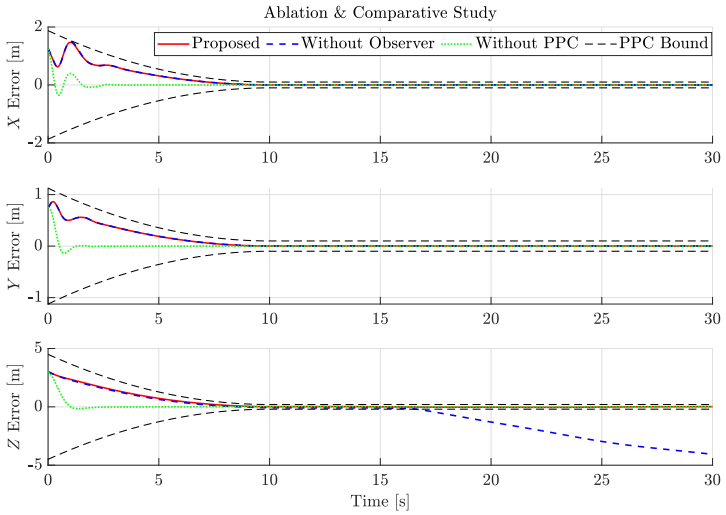

Figure 4. Comparative evolution of UAV tracking errors. Black dashed lines indicate PPC boundaries. UAV: Unmanned aerial vehicle; PPC: prescribed performance control.

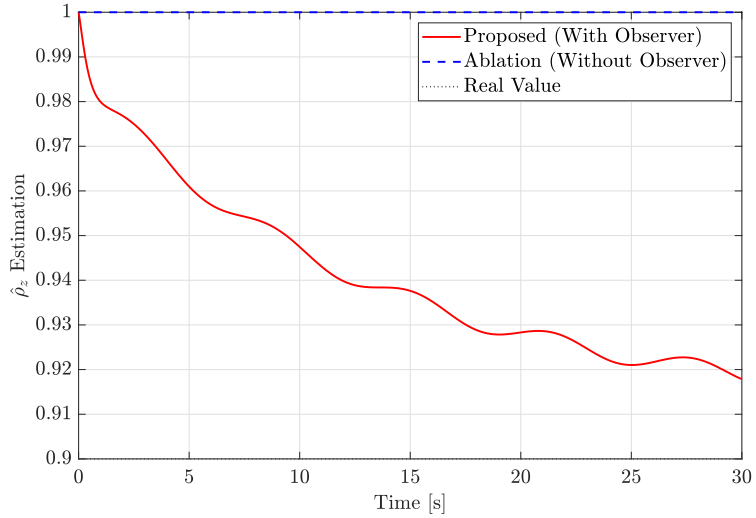

Figure 5. Adaptive estimation of UAV actuator efficiency ρ_z. UAV: Unmanned aerial vehicle.

Observer case (blue) diverges significantly after $t = 15$ s, eventually violating the PPC boundary. This proves that without the adaptive observer, even the PPC mechanism cannot prevent system failure under persistent actuator faults.

5.4. UAV parameter identification

Figure 5 illustrates the performance of the observer. For the **Proposed** case, the efficiency estimate $\hat{\rho}_z$ successfully converges from 1.0 to approximately 0.915, closely tracking the true fault value of 0.9. The small residual error is due to the robust σ-modification. In contrast, the **Ablation** case (blue) remains at 1.0, indicating that the actuator degradation cannot be detected. As shown in Figure 6, the bias estimate $\hat{c}$ does not exhibit divergence or saturation and stabilizes around -0.06. Although there is a steady-state deviation from the set true value of 0.05, this is acceptable in adaptive control theory. Due to the parameter redundancy among ρ, c, and d, the con-

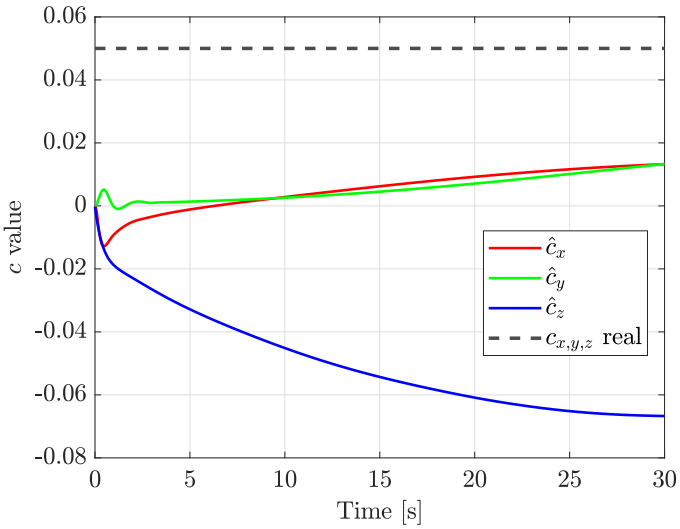

Figure 6. Estimation of UAV actuator bias faults ($\hat{c}$). UAV: Unmanned aerial vehicle.

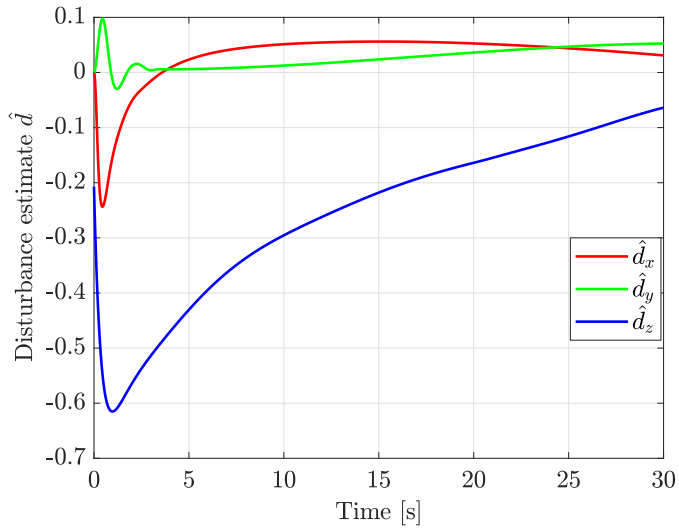

Figure 7. Estimation of lumped disturbances ($\hat{d}$) affecting the UAV. UAV: Unmanned aerial vehicle.

troller compensates for the overall error through coordinated adjustments of these parameters (e.g., a slightly higher $\hat{\rho}$ accompanied by a lower $\hat{c}$). The estimated values remain bounded, ensuring the stability of the control system. Figure 7 is a critical graph to validate the accuracy of the physical model. The estimated values converge to approximately -0.1 (close to 0) rather than the gravitational acceleration component (-9.8). This result provides strong evidence that the gravity feedforward compensation in the controller is correct. Consequently, the observer is only responsible for estimating the minute air resistance and residual modeling errors, reflecting the high fidelity of the model.

Remark 5 (Comprehensive analysis on parameter estimation and control objectives):
As shown in Figure 6, the estimated bias c stabilizes at –0.06, which differs from the true injected value of 0.05. It is crucial to clarify that this deviation does not invalidate the physical meaning of the controller, nor does it affect the system stability. This phenomenon is explained from three main aspects:

First, regarding **parameter identifiability**, the bias fault c and the lumped disturbance d_a are dynamically coupled, as they affect the UAV system through the exact same control input channel. In standard adaptive control theory, strict convergence of multiple coupled parameters to their true physical values requires the system states to satisfy the persistently exciting (PE) condition. However, achieving PE typically necessitates injecting rich, high-frequency signals into the trajectory, which would cause severe and unacceptable chattering during actual UAV flight. Without the PE condition, individual parameters are not strictly identifiable.

Second, regarding the **reasonableness of the framework**, such non-convergence to true values is a standard and acceptable characteristic of robust adaptive control. The robust σ-modification applied in the adaptive update laws [Equations (49) and (50)] guarantees that estimates will not drift to infinity but remain strictly bounded. The adaptive mechanism and the disturbance observer collaboratively compensate for the *algebraic sum* of uncertainties. As shown in Figure 7, d_a converges to approximately –0.1. The overall dynamic compensation provided by the controller is $-0.06 + (-0.1) = -0.16$, which effectively neutralizes the true combined uncertainty acting on the system channel.

Finally, regarding the **control objective**, the primary goal of the proposed fixed-time PPC is trajectory tracking and ensuring that errors remain strictly within safety boundaries, rather than performing precise system parameter identification. The Lyapunov-based stability analysis in Section 4 theoretically proves that tracking stability and error constraints are guaranteed as long as the overall uncertainty is compensated and the estimation errors remain bounded, completely independent of whether individual parameters converge to their exact physical true values.

5.5. Performance of USV formation (fixed-time stability)

Figure 8 illustrates the position tracking error curves of the four USVs during the formation process. The initial position errors of the followers (about 5 m) quickly converge to zero within an extremely short time interval ($t < 3$ s). In the steady state, the position tracking error is on the order of 10^{-3} and the convergence process is smooth, without any oscillations. These results show that the proposed fixed-time control law achieves a high convergence speed, enabling the USV formation to complete reconfiguration and reach a stable formation-keeping state in less than 3 s.

Figures 9 and 10 display the estimation results of the disturbance observers for the USV position loop and velocity loop, respectively. For the position loop disturbance estimates [Figure 9], the observed values converge to the steady state within 5 s, effectively capturing environmental disturbances such as currents.

For the velocity loop disturbances [Figure 10], different USVs (e.g., USV1 *vs.* USV2) experience different linear velocities due to their positions in the inner and outer lanes of the formation during turning maneuvers, leading to varying hydrodynamic drag forces. The estimated disturbance curves accurately reflect this physical phenomenon, converging to distinct constant values (ranging between -1 and +1). This proves that the observer can precisely capture model uncertainties under different dynamic states.

It is worth noting that, to clearly verify the baseline convergence and steady-state tracking performance of the proposed disturbance observers, the environmental disturbances in this simulation case are primarily modeled as steady-state components (e.g., constant ocean currents and mean wind forces). As shown in the results, the proposed observers rapidly and accurately converge to these constant principal values, demonstrating excellent steady-state estimation performance. Validating the system's robustness against higher-frequency, violently fluctuating wave dynamics remains an important aspect of future real-world experiments.

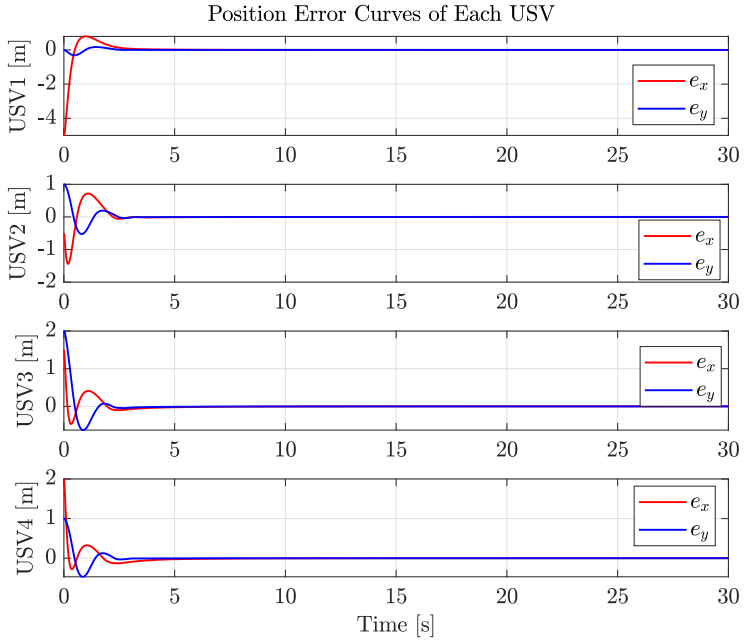

Figure 8. Convergence curves of position tracking errors for each autonomous vehicle. USV: Unmanned surface vehicle.

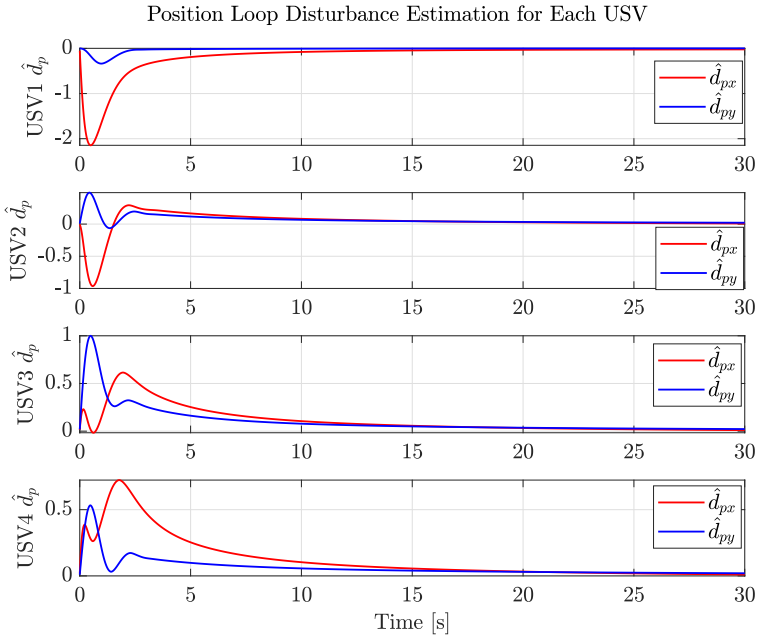

Figure 9. USV position loop disturbance estimation results. USV: Unmanned surface vehicle.

6. CONCLUSIONS

This study examines the issues related to robust cooperative control in heterogeneous UAV-USV systems and presents a novel fixed-time prescribed performance formation control structure for environments subject to actuator faults and nonlinear disturbances, based on fixed-time stability theory. In this theoretical context, a co-

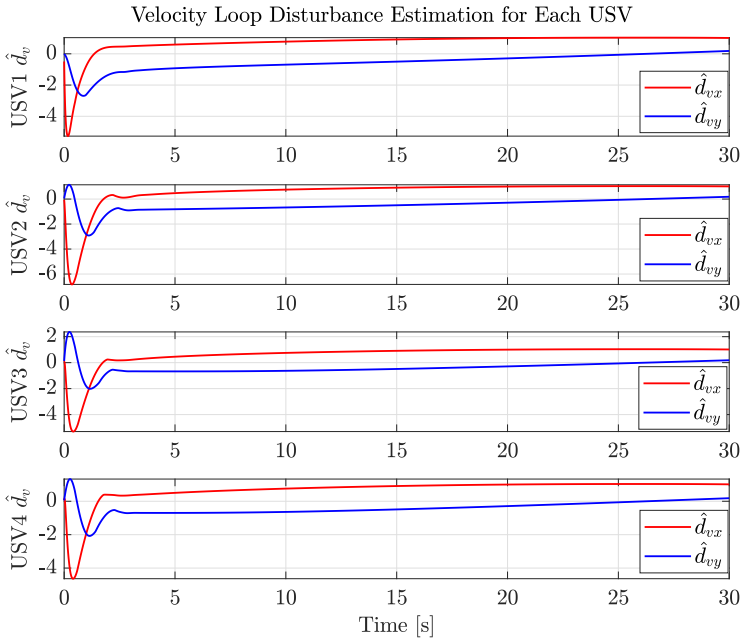

Figure 10. USV velocity loop disturbance estimation results. USV: Unmanned surface vehicle.

operative structure is developed by integrating the leader-follower topology for USV formation with prescribed performance constraints for UAV tracking. To improve control accuracy and convergence rate, a fixed-time control law based on a disturbance observer is employed to ensure that transient and steady-state errors converge within a certain time bound, irrespective of initial conditions. Furthermore, an adaptive fault-tolerant mechanism is implemented to precisely evaluate and compensate in real time for loss of actuator efficiency, bias faults, and lumped disturbances in heterogeneous agents. Simulation findings confirm the effectiveness of the suggested heterogeneous fixed-time prescribed performance formation control approach in maintaining precise formation geometry under dynamic conditions. Future work will extend the framework to address time-varying communication delays and packet losses within the proposed fixed-time stability analysis framework, with particular emphasis on experimental validation using physical UAV-USV systems in real maritime environments. In addition, simultaneous consideration of both abrupt and severe actuator failures in USVs and UAVs will be investigated in future studies.

DECLARATIONS

Authors' contributions

Made substantial contributions to the conception and design of the study and performed data analysis and interpretation: Liang, Z.; Zhou, W.; Wang, Y.

Performed data acquisition, as well as providing administrative, technical, and material support: Wang, Y.; Yang, Y.

Availability of data and materials

All simulation parameters and mathematical models used to support the findings of this study are included within the article.

AI and AI-assisted tools statement

During the preparation of this work, the authors used AI-assisted tools, specifically ChatGPT (version GPT-4, OpenAI), for language translation, text polishing to improve readability, and visual enhancement of block diagrams (e.g., layout optimization and formatting). The conceptual content, mathematical modeling, data generation, and all scientific results are entirely the original work of the authors. After using these tools, the authors thoroughly reviewed and edited both the manuscript and figures, and take full responsibility for the final content of the publication. No AI technologies were used in the study design, mathematical modeling, or generation of data and results.

Financial support and sponsorship

This work was supported by the National Natural Science Foundation of China (Grant Nos. 62203293 and 52407123) and the Social and People's Livelihood Science and Technology Project (Grant No. MSZ2025119).

Conflicts of interest

All authors declared that there are no conflicts of interest.

Ethical approval and consent to participate

Not applicable.

Consent for publication

Not applicable.

REFERENCES

1. Ren, H.; Liu, Q.; Zhou, Q.; Lu, R. A review of distributed cooperative control research on unmanned autonomous systems (in Chinese). *J. Guangdong Univ. Technol.* **2024**, *41*, 1–13. DOI
2. Xiong, Y.; Fu, M.; Li, B.; Yao, T.; Zhang, R. Multi-robot formation control based on leader-follower method (in Chinese). *Mech. Electr. Eng. Technol.* **2024**, *53*, 136–41. https://kns.cnki.net/kcms2/article/abstract?v=zE0--Q1IihSpR58jxWP-rI_Xt7XR2FFHu_0U64TvMTFY-xHgpaKYdipE-eFxbuLPGSU-Ef381kUv8Eb-Sohrv5y4Fntr8xVUXS49IIXdEAUhJXWsmxq3FSgyF7K9TbzRDnTjFc-J7R_WyHY983wtH9eT2GIu6MA-yHQIM3RsrXRywMCnN1Pw_w==&uniplatform=NZKPT&language=CHS. (accessed 2026-05-12)
3. Piracha, A. Z.; Rinner, B. Virtual leader-based safe formation-switching control for dense environments. In *ICASSP 2025 - 2025 IEEE International Conference on Acoustics, Speech and Signal Processing (ICASSP)*, Hyderabad, India. Apr 06-11, 2025. IEEE; 2025. p. 1-5. DOI
4. Luo, D.; Wang, Y.; Lewis, F. L.; Song, Y. Unified output feedback based prescribed performance consensus tracking control of heterogeneous multi-agent systems. *IEEE/CAA J. Autom. Sin.* **2025**, *12*, 1636–47. DOI
5. Wu, Y.; Low, K. H.; Lv, C. Cooperative path planning for heterogeneous unmanned vehicles in a search-and-track mission aiming at an underwater target. *IEEE Trans. Veh. Technol.* **2020**, *69*, 6782–7. DOI
6. Huang, T.; Chen, Z.; Gao, W.; Xue, Z.; Liu, Y. A USV-UAV cooperative trajectory planning algorithm with hull dynamic constraints. *Sensors* **2023**, *23*, 1845. DOI
7. Zhang, J.; Liu, X.; Wang, X.; Wang, Y.; Wang, Y. Adaptive prescribed performance tracking control for underactuated unmanned surface ships with input quantization. *Intell. Robot.* **2024**, *4*, 146–63. DOI
8. Li, J.; Zhang, G.; Zhang, X.; Zhang, W. Integrating dynamic event-triggered and sensor-tolerant control: application to USV-UAVs cooperative formation system for maritime parallel search. *IEEE Trans. Intell. Transp. Syst.* **2024**, *25*, 3986–98. DOI
9. Li, J.; Zhang, G.; Wang, L.; Zhang, X. Modeling and cooperative path following control of USVs-UAVs via the event-triggered communication. In *2024 36th Chinese Control and Decision Conference (CCDC)*, Xi'an, China. May 25-27, 2024. IEEE; 2024. pp. 1568-72. DOI
10. Li, X.; Cai, G.; Wu, T.; Yang, Q. A formation transformation control method for UAV swarm based on stress matrix (in Chinese). *Control Decis.* **2024**, *39*, 2195–204. DOI
11. Roggi, G.; Gozzini, G.; Invernizzi, D.; Lovera, M. Vision-based air-to-air autonomous landing of underactuated VTOL UAVs. *IEEE/ASME Trans. Mechatronics* **2024**, *29*, 2338–49. DOI

12. He, X.; Li, Y.; Yu, Y. Prescribed-time formation control of quadrotor UAVs based on leader-follower approach (in Chinese). *Control Eng. China* **2025**, *32*, 1813-21. DOI
13. Li, X.; Wen, G.; Sun, C. Leader-following consensus of open multi-unmanned aerial vehicles systems under directed topology. In *2024 SICE Festival with Annual Conference (SICE FES)*, Kochi City, Japan. Aug 27-30, 2024. IEEE; 2024. pp. 752-7. https://ieeexplore.ieee.org/document/10805206. (accessed 2026-05-12)
14. Sun, Y.; Peng, S. Consensus of discrete-time leader-following linear multi-agent systems under Lyapunov-function-based event-triggered mechanism. *IEEE Trans. Circuits Syst. II Exp. Briefs* **2023**, *70*, 4409–13. DOI
15. Song, S.; Liu, Z.; Yuan, S.; Wang, Z. Cascaded extended state observers-based fixed-time line-of-sight path following control for unmanned surface vehicles with disturbances and saturation. *IEEE Trans. Veh. Technol*. **2024**, *73*, 7733–47. DOI
16. Gao, H.; Xia, Y.; Liu, K.; Zhang, J.; Cui, B. Resilient neuroadaptive distributed fixed-time attitude coordination control for multiple spacecraft. *IEEE Trans. Cybern*. **2024**, *54*, 4973–85. DOI
17. Wang, T.; Xu, Y.; Liu, Y.; Wang, D. Fast fixed-time-synchronized sliding mode formation control for uncertain autonomous surface vehicles. In *2025 37th Chinese Control and Decision Conference (CCDC)*, Xiamen, China. May 16-19, 2025. IEEE; 2025. pp. 1664-9. DOI
18. Zhang, J.; Yu, S.; Yan, Y.; Wu, D. Fixed-time output feedback sliding mode tracking control of marine surface vehicles under actuator faults with disturbance cancellation. *Appl. Ocean Res*. **2020**, *104*, 102378. DOI
19. Shang, Y.; Ye, Y. Fixed-time group tracking control with unknown inherent nonlinear dynamics. *IEEE Access* **2017**, *5*, 12833–42. DOI
20. Shang, Y. Fixed-time group consensus for multi-agent systems with non-linear dynamics and uncertainties. *IET Control Theory Appl*. **2018**, *12*, 395–404. DOI
21. Sun, G.; Liang, B. Fixed-time observer based adaptive prescribed performance control for full state feedback system with disturbance. In *2024 IEEE 13th Data Driven Control and Learning Systems Conference (DDCLS)*, Kaifeng, China. May 17-19, 2024. IEEE; 2024. pp. 848-53. DOI
22. Peng, Y.; Yan, H.; Rao, K.; Yang, P.; Lv, Y. Distributed model predictive control for unmanned aerial vehicles and vehicle platoon systems: a review. *Intell. Robot*. **2024**, *4*, 293–317. DOI
23. Ding, J.; Zhang, H. T.; Hu, B. B.; Jiang, W.; Liu, X. Mutual-rendezvous control and feature-compatible landing optimization for heterogeneous UAV–USV fleets. *IEEE Trans. Ind. Inform*. **2026**, *22*, 348-59. DOI
24. Luo, Y.; Tang, F.; Wei, Q. Event-based human-in-the-loop formation-containment control for heterogeneous UAV-USV systems with dual predefined-time prescribed performance. *IEEE Trans. Veh. Technol*. **2026**, *75*, 1990-2000. DOI
25. Li, S.; Jia, Y.; Xiang, Z.; Zhang, J. Distributed event-triggered positive consensus protocol design for leader-following multi-agent systems. In *2025 IEEE 14th Data Driven Control and Learning Systems (DDCLS)*, Wuxi, China. May 09-11, 2025. IEEE; 2025. pp. 398-403. DOI
26. Su, W.; Mu, C.; Zhu, S.; Niu, B.; Sun, C. Event-triggered leader-follower bipartite consensus control for nonlinear multi-agent systems under DoS attacks. *Sci. China Inf. Sci*. **2025**, *68*, 132206. DOI
27. Wu, Y.; Liang, H.; Xuan, S.; Zhang, X. Extended state observer based finite-time fault-tolerant formation control for multi-UAVs. *J. Franklin Inst*. **2024**, *361*, 107158. DOI
28. Zhang, H.; Ding, Y.; Yue, X. Distributed formation control of aircraft with fixed-time and prescribed performance based on leader-follower approach (in Chinese). *Aeronaut. Sci. Technol*. **2025**, *36*, 1–9. DOI
29. Zheng, Z.; Wang, Y.; Li, C. Observer-based fixed-time leader-following consensus control for MASs subject to DoS attack. In *2023 7th International Symposium on Computer Science and Intelligent Control (ISCSIC)*, Nanjing, China. Oct 27-29, 2023. IEEE; 2023. pp. 236-40. DOI
30. Trejo, J. A. V.; Ponsart, J. C.; Adam-Medina, M.; Valencia-Palomo, G.; Theilliol, D. Distributed observer-based leader-following consensus control for LPV multi-agent systems: application to multiple VTOL-UAVs formation control. In *2023 International Conference on Unmanned Aircraft Systems (ICUAS)*, Warsaw, Poland. Jun 06-09, 2023. IEEE; 2023. p. 1-8. DOI
31. Yang, Y.; Shen, B.; Ge, X.; Li, S.; Han, Q. L. Dynamic event-triggered cluster consensus of multi-agent systems via PSO-GA co-design. *IEEE Trans. Autom. Sci. Eng*. **2025**, *22*, 11505–18. DOI
32. Yang, T.; Lu, Z.; Cui, G.; Ding, S. Funnel-based predefined-time formation control for heterogeneous vehicle platoon with asymptotic tracking. *IEEE Trans. Veh. Technol*. **2025**, *74*, 7178–87. DOI
33. Ballotta, L.; Talak, R. Safe distributed control of multi-robot systems with communication delays. *IEEE Trans. Veh. Technol*. **2025**, *74*, 10137–50. DOI
34. Wang, H.; Wang, H.; Guo, X. Distributed adaptive fault-tolerant formation control for heterogeneous USV-AUV swarms based on dynamic event triggering. *J. Mar. Sci. Eng*. **2025**, *13*, 2116. DOI
35. Ma, Y.; Jiang, B.; Wang, J.; Gong, J. Adaptive fault-tolerant formation control for heterogeneous UAVs-UGVs systems with multiple actuator faults. *IEEE Trans. Aerosp. Electron. Syst*. **2023**, *59*, 6705–16. DOI
36. Yang, Z.; Li, M.; Yu, Z.; Cheng, Y.; Xu, G.; Zhang, Y. Fault detection and fault-tolerant cooperative control of multi-UAVs under actuator faults, sensor faults, and wind disturbances. *Drones* **2023**, *7*, 503. DOI
37. Yang, Y.; Zhang, B.; Hu, M. Heterogeneous formation control of UAV-USV under actuator faults (in Chinese). *Flight Control Detect*. **2024**, *7*, 14–20. DOI
38. Charitidou, M.; Dimarogonas, D. V. Virtual leader and distance based formation control with funnel constraints. *IEEE Trans. Control Netw. Syst*. **2025**, *12*, 1342-53. DOI
39. Imran, I. H.; Kurtulus, D. F.; Memon, A. M.; Goli, S.; Kouser, T.; Alhems, L. M. Distributed robust formation control of heterogeneous

multi-UAVs with disturbance rejection. *IEEE Access* **2024**, *12*, 55326–41. DOI

40. Zhang, J.; Yu, S.; Yan, Y.; Zhao, Y. Fixed-time trajectory tracking control for marine surface vessels based on fixed-time disturbance observer. In *2020 5th International Conference on Automation, Control and Robotics Engineering (CACRE)*, Dalian, China. Sep 19-20. 2020. IEEE; 2020. pp. 308-12. DOI